

Mixed-salt effects on the conformation of a short salt-bridge-forming α helix: A simulation studyHao Shen,^{1,2} Wei Cheng,^{1,2} and Feng-Shou Zhang^{1,2,3,*}¹*The Key Laboratory of Beam Technology and Material Modification of Ministry of Education, College of Nuclear Science and Technology, Beijing Normal University, Beijing 100875, China*²*Beijing Radiation Center, Beijing 100875, China*³*Center of Theoretical Nuclear Physics, National Laboratory of Heavy Ion Accelerator of Lanzhou, Lanzhou 730000, China*

(Received 8 November 2013; revised manuscript received 19 January 2014; published 21 February 2014)

The structure of a single alanine-based ACE-AEAAAKEAAKA-NH₂ peptide in explicit aqueous solutions with mixed inorganic salts (NaCl and KCl) is investigated by using molecular simulations. The concentration of Na⁺, c_{Na^+} , varies from 0.0M to 1.0M, whereas the concentration of K⁺ is $1 - c_{\text{Na}^+}$. The simulated peptide is very sensitive to the change of concentration ratio between Na⁺ and K⁺. When the concentration ratio between Na⁺ and K⁺ is changed from 0.5/0.5, the structure of the peptide becomes loose or disordered. This specific phenomenon is confirmed via checking the changes of helix parameters and mapping the free energy along different coordinates. The higher normalized probability of forming direct and indirect salt bridges between residues Glu7⁻ and Lys11⁺ and the smallest probability of forming ringlike structures should be responsible for the stabilized helix structure in the 0.5 Na⁺/0.5 K⁺ solution. Furthermore, a noticeable conformational transition from an extended helix to an α helix is found in the 0.5 Na⁺/0.5 K⁺ solution, where a local ion cloud shows that some Na⁺ ions in the inner shells are still directly binding with the peptide, while K⁺ in the outer shells are moving into the inner shells, keeping the peptide in the collapsed state.

DOI: [10.1103/PhysRevE.89.022717](https://doi.org/10.1103/PhysRevE.89.022717)

PACS number(s): 87.15.kr, 87.15.hp

I. INTRODUCTION

Protein conformational changes play a key role in enzymatic catalysis, ligand binding, folding, protein lesions, and other processes involved in physiological function [1]. Several kinds of diseases that have not been solved so far are all related to the structural changes of protein, including Alzheimer's disease, Parkinson's disease, and type 2 diabetes mellitus [1–3]. Most biological molecules in complex aqueous environments, containing a significant amount of dissolved ions, show totally different phenomena [4]. It has been known that the added salt ions significantly affect the structural, thermodynamic properties of polypeptides, even their physiological functions [4,5]. Especially for the fundamental body-related ions, they are always involved in the specific and nonspecific physicochemical processes such as the solvent viscosity [6–8], (de)stabilizing of proteins, even nucleic acids [9], and surface tension [10,11]. Among the body-related ions, Na⁺ and K⁺, which are well known to play key roles in the stabilization and structural polymorphism of proteins, have long been studied both theoretically [12–17] and experimentally [18–20]. Series studies [12,13] showed that the strong direct ion binding of Na⁺ versus K⁺ to the proteins is caused by the larger charge density, resulting in an incline of the protein surface. It has also been suggested by experiments that the presence of divalent cations (Mg²⁺ and Cu²⁺) can greatly increase the helical content of ionized proteins [21,22]. In fact, even in a simple natural cell, five to ten types of inorganic compounds are contained. The structural changes induced by mixed inorganic salts are highly complex issues, which have not been investigated widely. Therefore, a thorough investigation of the possible mechanisms of the

conformational changes in hydrated inorganic salt solutions at different ratios is still necessary.

Since different ions have different effects on maintaining ordered or disordered protein structures, it is important to consider the competition of the distribution of different ions. In general, these distributions result from a balance of a terms of competing interactions such as competition between different ion-solute, ion-water, and ion-ion interactions. There are several mechanisms concerning the relationship between ions and solute. For example, the Debye-Hückel screening effect [23], which is dominated by the electrostatic potential among ions and charged groups of proteins, is measured as a function of Debye length [24]. Referring to the homogenous alkali-metal ions, the Debye length is nearly the same, resulting in little difference of the Debye-Hückel screening effect. Another popular theory indicates that the protein-ion interactions can be divided into two major mechanisms: the direct and indirect ion bindings [25]. The direct ion binding can affect the structures of hydration shells around particular residues through directly interacting with the polar groups, while the indirect ion binding can (de)stabilize the macromolecules' conformation by disrupting or regularizing the structure of surrounding water molecules. Regarding the ion-water interactions, the magnitude of ionic hydrated energy could consequently affect the direct or indirect binding to solute, in accordance with the law of matching water affinities [26,27]. For example, the properties of structure making of Na⁺ and structure breaking of K⁺ are discussed in Ref. [28]. As for the ion-ion interactions, the Lennard-Jones potential and Coulomb interactions are the majorities. In some solutions, ion clusters, resulting in a high solution viscosity, are usually generated via synergistic actions between different types of ions and water molecules, while for the Hofmeister series [28–30] they are the comprehensive results from all of the different inherent effects above.

Among the types of local structure in proteins, the α helix is the most regular and the most predictable from the

*Corresponding author: fszhang@bnu.edu.cn

sequence, as well as the most prevalent. The α helix is mainly stabilized by $(n, n + 4)$ backbone hydrogen bonds involving four amino acids per turn. It is said that the majority of short isolated helices derived from protein are unstable in an aqueous environment, unless stabilized by specific internal side-chain interactions, and alanine-based helices can hold the intrinsic helix well [31–34]. According to this theoretical hypothesis, Marqusee *et al.* [31] introduced a very instructive alanine-based peptide implanted with $(n, n + 4)$ salt bridged by residues Glu⁻ and Lys⁺, exhibiting a stable helix structure at $pH = 7.0$. Furthermore, this peptide is very sensitive to the subtle changes of the solution environment and provides an ideal model peptide for studying its reversible structural responses to mixed inorganic salts at different concentration ratios [13].

As for the physiological concentration around $0.15M$, the ion-induced effects are subtle and whether the conformational changes are induced by the foreign ions or the intrinsic characteristics is difficult to distinguish. Therefore, using a strong ionic strength of $1M$ is helpful to amplify the ion-induced effects [13]. Furthermore, a short peptide is always unstable in water solution. The conformational changes of the peptide are obvious by using a strong ionic strength instead of random changes in the physiological range. This is also convenient for counting the data for the peptide at different states. Regarding the Na⁺/K⁺ distributions, it is difficult to conclude whether or not a biological significance of the specific distributions exists. Furthermore, relevant research on this subject is deficient. In our present work, concentration-ratio-related conformational changes are noted and discussed. We believe further theoretical and experimental research is still urgently needed.

In this work, molecular dynamics simulation, which has been proved to be a useful method of discovering flexibility and tracing conformational changes at an atomic level [35–37], is used to reproduce the systems containing both Na⁺ and K⁺ ions and the simulation can show some interesting subtle results that cannot be proved by experiments [38]. The averaged peptide structures induced by mixed inorganic salts are compared and the competition between the two cations is investigated as the concentration ratio changes. Particular attention is focused on peptide structural stabilization mechanisms.

After the introduction, the model of the solvent molecule, the peptide model and ions, and the simulation method are explained in Sec. II. In Sec. III, our results are demonstrated and discussed. A summary is given in Sec. IV.

II. THEORY AND SIMULATION DETAILS

The peptide model of an alanine-based α helix, ACE-AEAAAKEAAKA-NH₂, is chosen as the starting structure in each simulation. This short-peptide model is extensively studied because of its biological importance as a basic ingredient of the salt-bridged stable structure, which can fundamentally reflect the responses to the mixture of different inorganic salts. The initial conformation of this peptide is created by MOLDEN software [39], corresponding to a segment of an ideal α -helix structure. Because of the instability of the short isolated helices, the acetyl (ACE) and amino (NH₂) are capped in order to make the peptide at a fully folded state.

The intermolecular energy consists of two parts: $E = E_{LJ} + E_C$, where E_{LJ} is the Lennard-Jones interac-

tion and E_C is the Coulomb interaction. They are expressed as

$$E_{LJ}(i, j) = 4\epsilon_{ij} \left[\left(\frac{\sigma_{ij}}{r_{ij}} \right)^{12} - \left(\frac{\sigma_{ij}}{r_{ij}} \right)^6 \right], \quad (1)$$

$$E_C(i, j) = \frac{q_i q_j}{4\pi \epsilon_0 r_{ij}}, \quad (2)$$

where ϵ_0 is the vacuum permittivity and r_{ij} the distance between two atoms. For the Lennard-Jones interaction, the first term is the short-range repulsion for molecules or atoms being too close to each other and the attraction, owing to the dispersion forces, is described in the second term. The OPLSAA-2001 fully atomistic force field [40] is employed for the whole system. The force field parameters of Na⁺, K⁺, and Cl⁻ ions are selected as $\epsilon_{Na^+} = 0.0116$ kJ/mol and $\sigma_{Na^+} = 3.3305$ Å, $\epsilon_{K^+} = 0.00137$ kJ/mol and $\sigma_{K^+} = 4.9346$ Å, and $\epsilon_{Cl^-} = 0.4928$ kJ/mol and $\sigma_{Cl^-} = 4.4172$ Å, respectively. Regarding the water model, we use the extended simple point charge (SPC/E) parameters [41] as it is well known to perform well in describing the bulk properties. The hydrogen bonds are described and the local orientational structures are given by the Coulomb interactions between point charges [42,43].

The GROMACS 4.5.6 packages, which were developed for simulations of arbitrary mixtures of molecules and macromolecules in solutions, are used to perform molecular dynamics simulations [44,45]. Electrostatic interactions are dealt with by the particle mesh Ewald summation method [46]. The cutoff for this long-range interaction is 1.4 nm. The double time-step algorithm by Tuckerman and Berne [47] is implemented.

There is one peptide segment, 2242 SPC/E solvent molecules, and 42 alkali-metal ions in each cubic cell ($42 \times 42 \times 42$ Å³). The alkali-metal ions are added in by randomly substituting the same numbers of water molecules as well as the Cl⁻ co-ions with the relative concentration of Na⁺ ions c_{Na^+} ranging from $0.0M$ to $0.3M$ to $0.5M$ to $0.7M$ to $1.0M$ and the reverse for c_{K^+} : (i) 0 Na⁺ and 42 K⁺ (abbreviated as 0.0 Na⁺/ 1.0 K⁺), (ii) 12 Na⁺ and 29 K⁺ (0.3 Na⁺/ 0.7 K⁺), (iii) 21 Na⁺ and 21 K⁺ (0.5 Na⁺/ 0.5 K⁺), (iv) 29 Na⁺ and 12 K⁺ (0.7 Na⁺/ 0.3 K⁺), and (v) 42 Na⁺ and 0 K⁺ (1.0 Na⁺/ 0.0 K⁺), respectively. At the beginning, a constricted 100-ps *NVT* simulation is performed and the solvent molecules and ions begin to form outer shells around the peptide obtaining the preliminary balance. Then another 5-ns *NPT* simulation is performed to produce pre-equilibrium with all released degrees of freedom and to steady the temperature and pressure. Each simulated system is maintained at 1.0 bar and 300 K, that is, standard atmospheric pressure and room temperature, by coupling the system via the Berendsen thermostat [48]. After that, the following simulations of 200 ns are carried out for data collection. In order to be more consistent, runs of 200 ns of these different concentrations have been simulated twice.

III. RESULTS AND DISCUSSION

A. Structural analysis

First we comment on convergence in terms of the reliability of classical molecular dynamic simulations. A convergence

test of the sampled fraction of the available volume of peptide by Fedorov *et al.* [49] suggests that a 10-ns simulation is long enough for ions to efficiently sample the peptide in such isolated-peptide simulations. However, the convergence of the peptide's conformational sampling at every state is the crucial issue because of the goal of investigating the mixed-salt-induced conformational changes. Therefore, the root mean square coordinate deviation (RMSD) against simulation time is plotted in Fig. 1 for further checking. As shown in Fig. 1, the RMSDs in 0.5 Na⁺/0.5 K⁺, 0.7 Na⁺/0.3 K⁺, and 1.0 Na⁺/0.0 K⁺ basically reach fixed values. For the cases of 0.3 Na⁺/0.7 K⁺ and 0.0 Na⁺/1.0 K⁺, the RMSDs are still in an increasing process. Consequently, several time periods can be divided according to whether the RMSD is basically stable or around a specific value, for example, 0.0 Na⁺/1.0 K⁺ (30–50–130–200 ns), 0.3 Na⁺/0.7 K⁺ (30–50–175–200 ns), 0.5 Na⁺/0.5 K⁺ (30–50–150–200 ns), 0.7 Na⁺/0.3 K⁺ (30–50–200 ns), and 1.0 Na⁺/0.0 K⁺ (30–50–80–200 ns). For each time period, a simulation of at least 20 ns is carried out for conformational sampling. In addition, the protecting effect in the 0.5 Na⁺/0.5 K⁺ solution is significant for its smaller RMSD values (basically from 0.2 to 0.4 nm) and whether a folding process happened in the 0.3 Na⁺/0.7 K⁺ and 0.0 Na⁺/1.0 K⁺ solutions makes no difference to the finding of the best stabilized α helix in the 0.5 Na⁺/0.5 K⁺ solution. Further, the following smooth free-energy maps suggest enough conformational sampling for different states (shown in Fig. 3). In our work, we focus on the simulation time from 50 to 200 ns because of its much greater number of sampling conformations and obvious markups for different states. We do not aim to be quantitative on the structural changes, but focus on the discussion of underlying mechanisms.

As shown in Fig. 1, from the initial time to 50 ns, each simulated peptide reaches a relative equilibrium state with a smaller RMSD value close to the helix structure except for 0.7 Na⁺/0.3 K⁺, the value of which rises to 0.4 nm at this time period. After 50 ns, the RMSDs of the 0.0 Na⁺/1.0 K⁺ and 1.0 Na⁺/0.0 K⁺ cases first reach a state in which the RMSDs are nearly the same as before but with larger fluctuations and

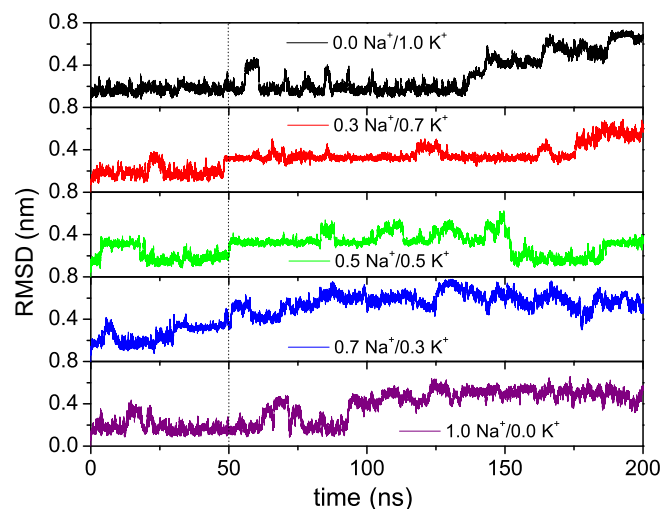


FIG. 1. (Color online) Root mean square coordinate deviation (RMSD) over the whole trajectory in each simulation.

then rise to 0.65 and 0.4 nm, respectively. The RMSD of 0.3 Na⁺/0.7 K⁺ is initially steady around a larger value of 0.4 nm and then rises to 0.6 nm. As for 0.7 Na⁺/0.3 K⁺, the RMSD increases to 0.6 quickly and swings back and forth around it. Compared with the quick unfolding processes in the 0.7 Na⁺/0.3 K⁺ solution, the increases of the RMSDs of 0.0 Na⁺/1.0 K⁺ (130–200 ns), 0.3 Na⁺/0.7 K⁺ (175–200 ns), and 1.0 Na⁺/0.0 K⁺ (80–200 ns) are very time consuming, especially for the 0.0 Na⁺/1.0 K⁺ and 1.0 Na⁺/0.0 K⁺ solutions for which the RMSD could stay around 0.2 for a long time. It is surprising that the RMSD of 0.5 Na⁺/0.5 K⁺ dramatically decreases after 150 ns. This is entirely different from other solutions' continually increasing trends. Averaged structures are also collected and shown in Fig. 2, according to their own time periods. The whole trajectory is first aligned to the initial structure to get the stacking traces and then the averaged peptide structure over each trajectory is extracted. As shown in Fig. 2, for the case of 0.7 Na⁺/0.3 K⁺, the peptide










Solution	Averaged Structures (Residue 1 → Residue 12)	
0.0 Na ⁺ /1.0 K ⁺	 (50–130 ns)	 (130–200 ns)
0.3 Na ⁺ /0.7 K ⁺	 (50–175 ns)	 (175–200 ns)
0.5 Na ⁺ /0.5 K ⁺	 (50–150 ns)	 (150–200 ns)
0.7 Na ⁺ /0.3 K ⁺	 (50–200 ns)	
1.0 Na ⁺ /0.0 K ⁺	 (50–80 ns)	 (80–200 ns)

FIG. 2. (Color online) Averaged structures at their own time periods after 50 ns. The left and right terminal groups of ACE and NH₂ are not included. The sequence of each structure is shown from residue 1 on the left to residue 12 on the right.

totally holds a random coil structure along the whole trajectory. For other cases, the peptide is closer to the original α helix at the first time period, although loop structures are found at the C terminal for the cases of $0.3 \text{ Na}^+/0.7 \text{ K}^+$ and $0.5 \text{ Na}^+/0.5 \text{ K}^+$. However, at the second time period, the α -helix structure can only be seen in the $0.5 \text{ Na}^+/0.5 \text{ K}^+$ solution. Compared with all the solutions, the peptide in the $0.5 \text{ Na}^+/0.5 \text{ K}^+$ solution is obviously found at the most stable α -helix state.

To further check this phenomenon, the four basic helix parameters are calculated and listed in Table I. According to the ideal helix, the amino acids are arranged in a right-handed helical structure where each amino acid residue corresponds to a 100° turn in the helix and a translation of 0.15 nm along the helical axis. What is most fundamental is that the N-H group of an amino acid forms a hydrogen bond with the C=O group of the amino acid four residues earlier; this repeated $(n, n+4)$ hydrogen bonding is the most prominent characteristic of an α helix. Therefore, the four structural parameters (H-bond distance, radius, rise, and twist) can generally display the conformational transitions of the peptide.

Consistent with previous results, the helix parameters in the $0.0 \text{ Na}^+/1.0 \text{ K}^+$ and $1.0 \text{ Na}^+/0.0 \text{ K}^+$ solutions are closer to the idea helix at the beginning and then the parameters deviate from the initial values quickly. However, the helix parameters in the $0.5 \text{ Na}^+/0.5 \text{ K}^+$ solution are mainly maintained near the ideal α -helix values. It is very interesting to note that when the concentration ratio changes from $0.5/0.5$ to $0.3/0.7$ or $0.7/0.3$, the helix parameters can suddenly deviate from the α -helix state. It seems that the peptide is very sensitive to the changes in concentration ratio between Na^+ and K^+ . Between the cases of $0.3 \text{ Na}^+/0.7 \text{ K}^+$ and $0.7 \text{ Na}^+/0.3 \text{ K}^+$, although the peptide in the $0.7 \text{ Na}^+/0.3 \text{ K}^+$ solution unfolds faster from the helical state, the final four helix parameters of the two cases are nearly the same, indicating the existence of unequally mixed ions resulting in a resistance for the folding process. Furthermore, the decrease of rise from 0.15 nm is found in the cases of the $0.0 \text{ Na}^+/1.0 \text{ K}^+$ and $1.0 \text{ Na}^+/0.0 \text{ K}^+$ solutions, in accordance with the formation of the ringlike structures (to be discussed later). It is said that the strong interaction of sodium with the backbone carbonyls can result in an intriguingly long-lived protein configuration in high-concentration salt solutions [13,50]. In our $1.0 \text{ Na}^+/0.0 \text{ K}^+$ solution, a ringlike coil structure is also found with a duration time of nearly 40 ns .

B. Free-energy landscape

A free-energy landscape has been commonly used to confirm the reaction paths of structural changes. Usually the coarse free energy is calculated from $\Delta G(X) = -K_B T \ln[P(X)]$ [13,51], where X is any set of reaction coordinates and the normalized probability $P(X)$ is generated according to the fully helical reference structure. Then the relative free energy can be easily expressed. Although the free energy is roughly estimated, the relative difference between different points is accurate. A comparative analysis is carried out by mapping the free-energy landscape along the radius of gyration (RG) and RMSD in Figs. 3(a) and 3(b), respectively. Here the root mean square coordinate deviation is

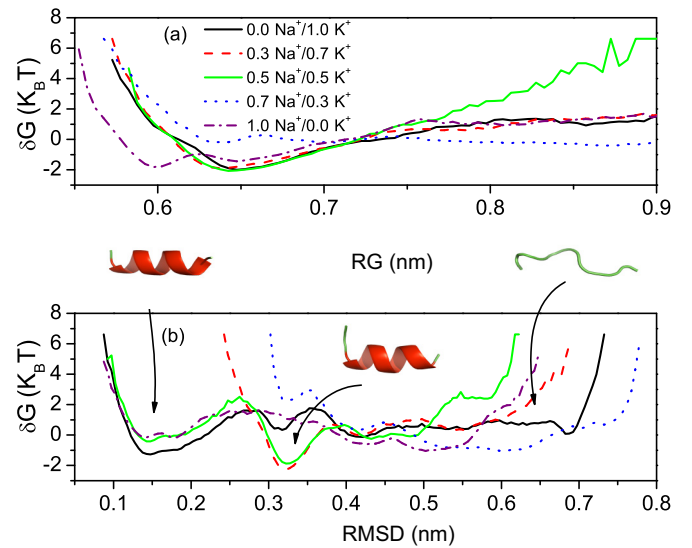


FIG. 3. (Color online) Coarse free-energy landscape along the different reaction coordinates (a) RG and (b) RMSD. The data are collected from 50 to 200 ns. The black solid line stands for $0.0 \text{ Na}^+/1.0 \text{ K}^+$, the red (dashed) line for $0.3 \text{ Na}^+/0.7 \text{ K}^+$, the green solid (light gray) line for $0.5 \text{ Na}^+/0.5 \text{ K}^+$, the blue (dotted) line for $0.7 \text{ Na}^+/0.3 \text{ K}^+$, and the purple (dash-dotted) line for $1.0 \text{ Na}^+/0.0 \text{ K}^+$.

defined as

$$r_{\text{RMSD}}(t_1, t_2) = \sqrt{\frac{1}{M} \sum_{i=0}^N m_i [\vec{r}_i(t_1) - \vec{r}_i(t_2)]^2}, \quad (3)$$

where $M = \sum_{i=0}^N m_i$, N is the number of atoms of the whole system, and $r_i(t)$ is the position of atom i at time t . The radius of gyration is defined as

$$r_{\text{RG}} = \sqrt{\frac{1}{M} \sum_{i=0}^N (\vec{r}_i)^2 (m_i)}, \quad (4)$$

where $M = \sum_{i=0}^N m_i$, m_i is the mass of atom i , and r_i is the position of atoms i with respect to the center of mass of the peptide. The distribution in Fig. 3(a) is very simple with an obvious minimum at a RG equal to 0.64 nm , suggesting that a compact movement occurs in each case except for the $0.7 \text{ Na}^+/0.3 \text{ K}^+$ solution, in which the peptide mostly exhibits a random coil structure. Regarding the free energy in Fig. 3(b), three distinct minima are shown in the $0.10\text{--}0.20$, $0.30\text{--}0.35$, and $0.50\text{--}0.70$ domains, respectively. For each separate domain, a representative conformation is extracted according to the corresponding value of the RMSD: the α helix for the RMSD between 0.1 and 0.2 nm , the extended helix for the RMSD between 0.30 and 0.35 nm , and the random coil for the RMSD between 0.5 and 0.7 nm . This is consistent with the averaged structures for each case in Fig. 2. Compared with the monotonic changes along the RG, the coarse free energy along the RMSD can exhibit more detailed information, such as the α -helix state and the extended helix state. Therefore, a comprehensive comparative analysis along different reaction coordinates is necessary to get accurate information about the conformational transformation. As shown in Fig. 3(b), for the

TABLE I. Four helix parameters in different solutions. For the helix parameters, the H-bond distance is defined as the most prominent characteristic of repeated $(n, n + 4)$ hydrogen bonding in an α helix, “Radius” denotes the radius of curvature, “Rise” is the positional translation along the helical axis, and “Twist” is the angular translation along the helical axis in each case. The b_i and e_i represent the averaged structure time periods discussed above. For example, b_1 stands for 50–130 ns, e_1 for 130–200 ns, b_2 for 50–175 ns, e_2 for 175–200 ns, b_3 for 50–150 ns, e_3 for 150–200 ns, b_4 for 50–80 ns, and e_4 for 80–200 ns.

Solutions	H-bond distance (nm)	Radius (nm)	Rise (nm)	Twist (degree)
ideal helix	0.30	0.23	0.15	100
0.0 Na ⁺ /1.0 K ⁺ _{<i>b</i>1}	0.36 ± 0.05	0.23 ± 0.01	0.16 ± 0.01	99.28 ± 4.78
0.0 Na ⁺ /1.0 K ⁺ _{<i>e</i>1}	0.67 ± 0.19	0.30 ± 0.05	0.13 ± 0.05	56.06 ± 37.69
0.3 Na ⁺ /0.7 K ⁺ _{<i>b</i>2}	0.41 ± 0.05	0.26 ± 0.02	0.15 ± 0.02	88.18 ± 8.31
0.3 Na ⁺ /0.7 K ⁺ _{<i>e</i>2}	0.81 ± 0.11	0.32 ± 0.05	0.18 ± 0.05	48.60 ± 28.71
0.5 Na ⁺ /0.5 K ⁺ _{<i>b</i>3}	0.44 ± 0.07	0.27 ± 0.02	0.14 ± 0.21	83.89 ± 13.10
0.5 Na ⁺ /0.5 K ⁺ _{<i>e</i>3}	0.38 ± 0.06	0.24 ± 0.02	0.15 ± 0.01	95.15 ± 11.31
0.7 Na ⁺ /0.3 K ⁺	0.86 ± 0.13	0.31 ± 0.06	0.18 ± 0.06	49.83 ± 27.13
1.0 Na ⁺ /0.0 K ⁺ _{<i>b</i>4}	0.39 ± 0.06	0.23 ± 0.01	0.16 ± 0.01	96.95 ± 6.66
1.0 Na ⁺ /0.0 K ⁺ _{<i>e</i>4}	0.57 ± 0.12	0.29 ± 0.04	0.12 ± 0.05	68.53 ± 22.74

cases of the 0.0 Na⁺/1.0 K⁺ and 1.0 Na⁺/0.0 K⁺ solutions, the magnitudes of the two minima are nearly the same, so there should be a strong competition of the conformational transitions between the α -helix and random coil states in these solutions. When 0.3M K⁺ is replaced by Na⁺, the extended helix structure becomes the favorable conformation and the α -helix state disappears. For the 0.5 Na⁺/0.5 K⁺ solution, it is surprising to see that not only does the α -helix state appear again, but also the free energy in the second domain still exists. Although the relative free-energy difference between the two local minima is nearly $1.5K_B T$, the reverse conformational transition from the extend helix state to the α -helix state is confirmed via checking the averaged structures along the simulation time. Further adding Na⁺ to 0.7M would suddenly make the peptide stay at the random coil state. Above all, both the α -helix and random coil states exist in the 0.5 Na⁺/0.5 K⁺ solution; furthermore, the noticeable conformational transition from the extended helix state to the α -helix state is found. This is consistent with the change of helical parameters in Table I, indicating the characteristic protecting effect playing a large role in the 0.5 Na⁺/0.5 K⁺ physiological environment.

For a clear understanding of the conformational transition, the two-dimensional free-energy maps are also plotted in

Fig. 4. The arrows are drawn according to the change of the RMSD with the simulation time. As shown in Fig. 4, the obvious folding process from the extended helix state to the α -helix state is seen in the case of the 0.5 Na⁺/0.5 K⁺ solution. Although a more stable α -helix state is formed in the 0.0 Na⁺/1.0 K⁺ and 1.0 Na⁺/0.0 K⁺ solutions, the unfolding processes along the changes of the RMSD are, however, unavoidable. The added foreign ions change these unfolding processes in that the preferred extended helix state in the 0.3 Na⁺/0.7 K⁺ solution, the α -helix state in the 0.5 Na⁺/0.5 K⁺ solution, and the random coil state in the 0.7 Na⁺/0.3 K⁺ solution are all distinct from the situations in the single-cation solutions.

C. Salt-bridge-forming and ringlike structures

The α helix is mainly stabilized by $(n, n + 4)$ backbone hydrogen bonds involving four amino acids per turn. As an alanine-based α -helix peptide model of ACE-AEAAAKEAAKA-NH₂, with the two salt bridges between charged residues Glu2⁻ and Lys6⁺, residues Glu7⁻ and Lys11⁺ can directly stabilize the α -helix structure by shifting the helix to more compact structures [52] and additionally may

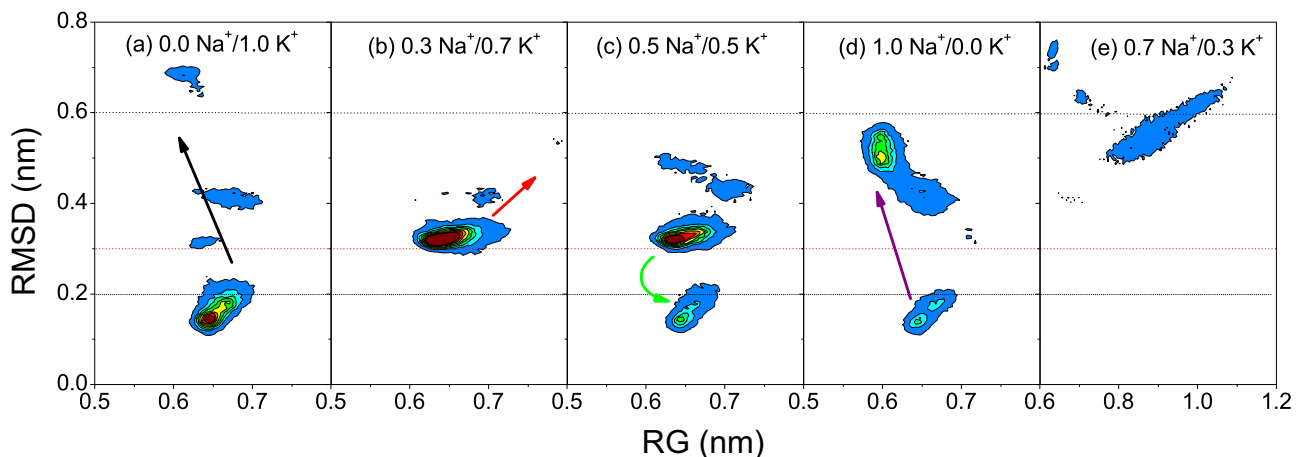


FIG. 4. (Color online) Two-dimensional free-energy maps along the RG and RMSD in each solution. The arrows are drawn according to the change of RMSD with simulation time. The data are collected from 50 to 200 ns.

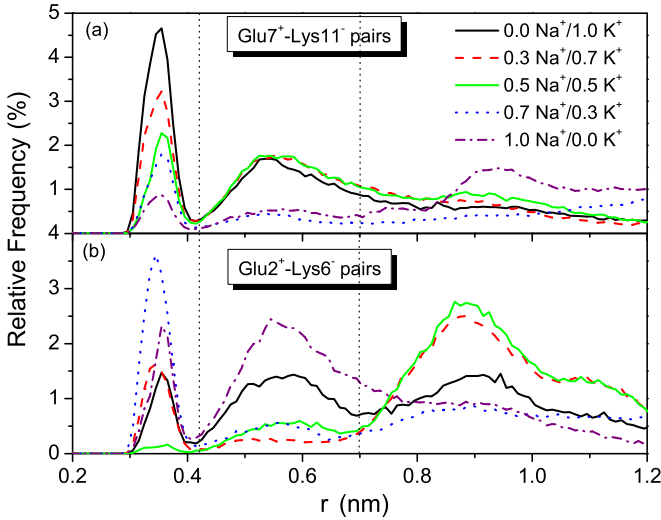


FIG. 5. (Color online) Normalized probability distribution of distance between carboxylate carbon atom on Glu^- and the amine nitrogen atom on Lys^+ for the (a) second and (b) first salt bridges. The data are collected from 50 to 200 ns. The black solid line stands for $0.0 \text{ Na}^+/1.0 \text{ K}^+$, the red (dashed) line for $0.3 \text{ Na}^+/0.7 \text{ K}^+$, the green solid (light gray) line for $0.5 \text{ Na}^+/0.5 \text{ K}^+$, the blue (dotted) line for $0.7 \text{ Na}^+/0.3 \text{ K}^+$, and the purple (dash-dotted) line for $1.0 \text{ Na}^+/0.0 \text{ K}^+$.

contribute to the helix stability by backbone desolvation and shielding from water molecules [53,54]. Here the normalized probability distribution of $P(r)$, where r is the distance between the carboxylate carbon atom on Glu^- and the amine nitrogen atom on Lys^+ for the first and second salt bridges, is averaged over the trajectory after 50 ns and shown in Fig. 5.

As Joachim mentioned in Ref. [13], there are two major types of salt bridge in Glu^- - and Lys^+ -based peptides. One is the first peak for $r \leq r_d \approx 0.42 \text{ nm}$, indicating a direct salt bridge; the other is the second peak for $r_d \leq r \leq r_{id} \approx 0.70 \text{ nm}$, corresponding to an indirect salt bridge separated by one or two water molecules. When $r \geq 0.70 \text{ nm}$, the residues Glu^- and Lys^+ are unrelated and free to be contacted by other water molecules or ions. As shown in Fig. 5(a), an increased probability of forming a direct or indirect salt bridge for the Glu7-Lys11 pair is seen when the concentration ratio linearly changes from $1.0 \text{ Na}^+/0.0 \text{ K}^+$ to $0.0 \text{ Na}^+/1.0 \text{ K}^+$. It seems that the strong interaction of Na^+ makes it difficult to form a salt bridge between Glu7 and Lys11 . The situation for the Glu2-Lys6 pair is more complicated in Fig. 5(b). Although the probability of forming a Glu7-Lys11 pair is smaller for the cases of $0.7 \text{ Na}^+/0.3 \text{ K}^+$ and $1.0 \text{ Na}^+/0.0 \text{ K}^+$, the direct and indirect salt bridges are easily formed between residues Glu2^- and Lys6^+ . The highest normalized probability of the direct salt bridge is found in the $0.7 \text{ Na}^+/0.3 \text{ K}^+$ solution, about 3.79% at 0.35 nm, however, with the averaged random coils along the whole simulation. Meanwhile, in the $0.5 \text{ Na}^+/0.5 \text{ K}^+$ solution, the unrelated state is the dominant interrelationship for the Glu2-Lys6 pair.

For a better understanding, we integrate r from 0.0 to r_d or r_{id} in Table II to find whether a direct or indirect salt bridge is formed in our simulations by $p(r_j) = \int_0^{r_j} P(r) dr$, where $j = d$ or id , respectively. As shown in Table II, for the

TABLE II. Normalized probability (%) of forming the first salt bridge ($sb1$) and second salt bridge ($sb2$) in different solutions.

Solutions	$p_{sb1}(r_d)$	$p_{sb1}(r_{id})$	$p_{sb2}(r_d)$	$p_{sb2}(r_{id})$
$0.0 \text{ Na}^+/1.0 \text{ K}^+$	7.89	37.24	27.74	60.78
$0.3 \text{ Na}^+/0.7 \text{ K}^+$	9.58	16.13	19.55	56.27
$0.5 \text{ Na}^+/0.5 \text{ K}^+$	1.04	12.72	12.35	49.49
$0.7 \text{ Na}^+/0.3 \text{ K}^+$	20.64	31.36	10.21	18.68
$1.0 \text{ Na}^+/0.0 \text{ K}^+$	11.82	58.82	5.31	16.93

Glu7-Lys11 pair, a slight linear increase of probability from 16.93% to 60.78% is expressed when the concentration of Na^+ decreases from $1.0M$ to $0.0M$, suggesting that replacing Na^+ by K^+ can consequently increase the chances of forming salt bridges between residues Glu7^- and Lys11^+ , shielding the backbone from solvation. Regarding the Glu2-Lys6 pair, by either replacing $0.3M \text{ K}^+$ by Na^+ or replacing $0.3M \text{ Na}^+$ by K^+ , a higher probability of the direct salt bridge and a smaller probability of the indirect salt bridge are found. It seems that the unequally mixed inorganic ions can enhance the chance of forming direct salt bridges and reduce the chance of forming indirect ones between the Glu2-Lys6 pair.

Why are the conditions of the two pairs so different? Although the surroundings and component parts are nearly the same, the situations of the Glu2-Lys6 and Glu7-Lys11 pairs are completely different. This is mainly because of the local chemical polarity of the C terminal (apolar) and the N terminal (polar). For the Glu7-Lys11 pair near the N terminal, Na^+ is inclined to break this bond while K^+ protects this bond. As shown in Table II, more K^+ means greater probability of forming direct or indirect salt bridges. Regarding the Glu2-Lys6 pair near the C terminal, the larger helicity is found in solutions containing more Na^+ . Recall the rise parameter in Table I. The rise parameter along the simulation time is separately plotted in Fig. 6. The long-lived averaged structure of the specific rise (0.05 nm) also shows that the Glu2^- and

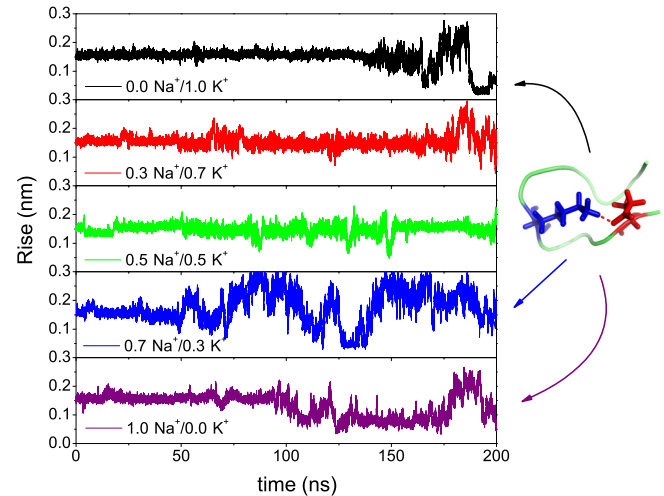


FIG. 6. (Color online) Rise parameter along simulation time in each case. The representative ringlike structure is shown on the right side. The salt bridge are significantly formed between the residues Glu2^- (right) and Lys6^+ (left).

Lys6⁺ are directly bonded. Here a hypothesis is posed that the decrease of the rise parameter is in accord with the existence of long-lived ringlike structures in the 1.0 Na⁺/0.0 K⁺ solution. It can be proposed that the peptide in 0.0 Na⁺/1.0 K⁺ might also go through such a conformational transition because of the similar decline of the rise parameter, although this transition is hard to notice because of its shorter duration time. As shown in Fig. 6, drops of the rise parameter to 0.05 nm can be seen in the 0.0 Na⁺/1.0 K⁺ (190–196 ns), 1.0 Na⁺/0.0 K⁺ (134–174 ns), and 0.7 Na⁺/0.3 K⁺ (127–132 ns) solutions. Because of the short duration time, only the first two cases can be noticed through the averaged rise parameter in Table I. The abundance of ringlike structures is in accord with the greater probability of forming direct or indirect salt bridges for the Glu2-Lys6 pair in the 0.0 Na⁺/1.0 K⁺ (37.24%), 0.7 Na⁺/0.3 K⁺ (31.36%), and 1.0 Na⁺/0.0 K⁺ (58.82%) solutions. It seems that the added single cations, especially for Na⁺, can consequently result in the conformational change to ringlike structures. Because of this, the α -helix state is unstable in the 0.0 Na⁺/1.0 K⁺, 0.7 Na⁺/0.3 K⁺, and 1.0 Na⁺/0.0 K⁺ solutions.

D. Local ion crowding

As mentioned by Xia *et al.* [55], for both the hen egg white lysozyme and protein L, a collapse of denatured protein is revealed in the high-concentration urea/GdmCl mixture. Here the word “collapse” means that proteins populate more compact structures. This collapse of protein is contributed to the decreased solubility and increased non-native self-interactions of hydrophobic residues, owing to the stronger electrostatic interactions of GdmCl with proteins and the enhanced local crowding of urea molecules around the protein surface. This local urea cloud around particular residues can result in an effective residue-residue interaction, especially for the apolar ones. To understand this stabilizing processes for the Na⁺/K⁺ mixture, the native contacts, non-native contacts, and accessible surface areas are investigated in Table III, where the accessible surface areas in the 0.0 Na⁺/1.0 K⁺, 0.3 Na⁺/0.7 K⁺, 0.7 Na⁺/0.3 K⁺, and 1.0 Na⁺/0.0 K⁺ solutions show basically increasing trends. Meanwhile, the decrease of native contacts and increase of non-native contacts exhibit a

TABLE III. Accessible surface area (ASA), native (protein-protein) contacts, and non-native (protein-nonprotein) contacts in different solutions. The contacts are defined within a cutoff of 0.35 nm. The *bi* and *ei* are the same as the time periods collected in Table I.

Solutions	ASA (nm ²)	Native contacts	Non-native contacts
0.0 Na ⁺ /1.0 K ⁺ _{bi}	12.07 ± 0.51	2332.5 ± 45.5	818.6 ± 53.9
0.0 Na ⁺ /1.0 K ⁺ _{ei}	12.89 ± 0.96	2237.2 ± 80.2	862.3 ± 71.3
0.3 Na ⁺ /0.7 K ⁺ _{b2}	11.97 ± 0.55	2331.2 ± 49.3	807.7 ± 56.0
0.3 Na ⁺ /0.7 K ⁺ _{e2}	14.05 ± 0.71	2143.2 ± 53.5	929.4 ± 61.3
0.5 Na ⁺ /0.5 K ⁺ _{b3}	12.14 ± 0.58	2320.6 ± 49.7	815.3 ± 55.9
0.5 Na ⁺ /0.5 K ⁺ _{e3}	12.04 ± 0.53	2333.1 ± 49.6	812.5 ± 56.2
0.7 Na ⁺ /0.3 K ⁺	14.03 ± 1.10	2150.7 ± 74.6	928.8 ± 77.6
1.0 Na ⁺ /0.0 K ⁺ _{b4}	12.25 ± 0.48	2317.6 ± 41.3	830.6 ± 52.6
1.0 Na ⁺ /0.0 K ⁺ _{e4}	12.28 ± 0.86	2287.5 ± 70.2	827.7 ± 70.3

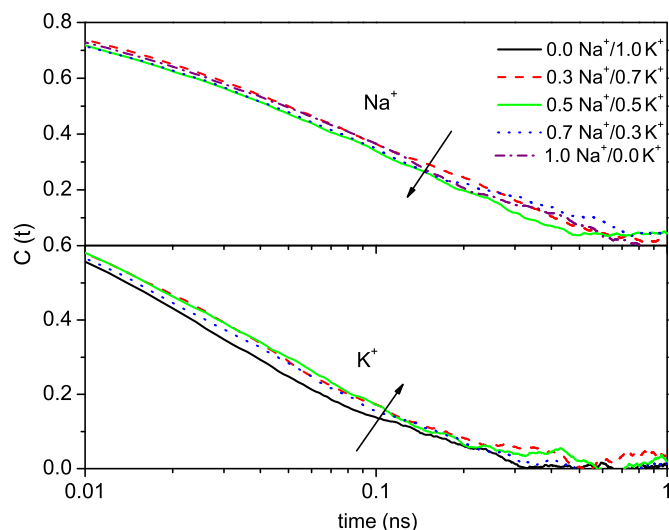


FIG. 7. (Color online) Autocorrelation functions about the numbers of local cations around the protein surface within a cutoff of 0.5 nm, on a log-linear plot from 0.01 to 1 ns. The numbers of cations are collected from 50 to 200 ns. The black solid line stands for 0.0 Na⁺/1.0 K⁺, the red (dashed) line for 0.3 Na⁺/0.7 K⁺, the green solid (light gray) line for 0.5 Na⁺/0.5 K⁺, the blue (dotted) line for 0.7 Na⁺/0.3 K⁺, and the purple (dash-dotted) line for 1.0 Na⁺/0.0 K⁺.

solvation process. In contrast to the above four cases, for the 0.5 Na⁺/0.5 K⁺ solution, the decrease of accessible surface areas and the increase of native contacts indicate that the collapsed state of proteins is achieved by the self-interactions. However, it is still slightly different from the situation in Ref. [55] in which the urea and GdmCl are both denaturants and there are also strong interactions between them.

To further analyze the process, the time-dependent numbers of local cations around the protein surface within a cutoff of 0.5 nm are collected from 50 to 200 ns and then its autocorrelation functions are plotted in Fig. 7. All the autocorrelation functions decrease from 1.0 at beginning, but, for a better understanding, the log-linear coordinates are used from 0.01 to 1 ns. As shown in Fig. 7, the curve of local K⁺ in the 0.5 Na⁺/0.5 K⁺ solution decreases much more slowly than that in other solutions while faster for that of Na⁺. This means that in the 0.5 Na⁺/0.5 K⁺ solution, the longest interaction time of K⁺ with protein is found and the shortest for that of Na⁺.

From the time-dependent radial distribution functions (50–200 ns) of cations to negatively charged (Glu) and uncharged residues (Ala) in Fig. 8, a significant decrease of Na⁺ at 0.32 nm for negative charged Glu⁻ is consistently seen while an increase for K⁺. This means that a few Na⁺ ions are excluded to the outer shells, while K⁺ moves inside. The crowding ion cloud of K⁺ and Na⁺ around the protein surface at about 0.32 nm can keep the peptide from interacting with polar water molecules. This is different from the results exhibited in Refs. [55,56] in which the stronger denaturants, such as GdmCl, always stay in the inner shells around the protein and bind with the polar groups along the whole simulation in higher concentrations. In our simulations, a number of Na⁺ ions are also excluded from the inner shells. For the uncharged residues, a subtle change is shown

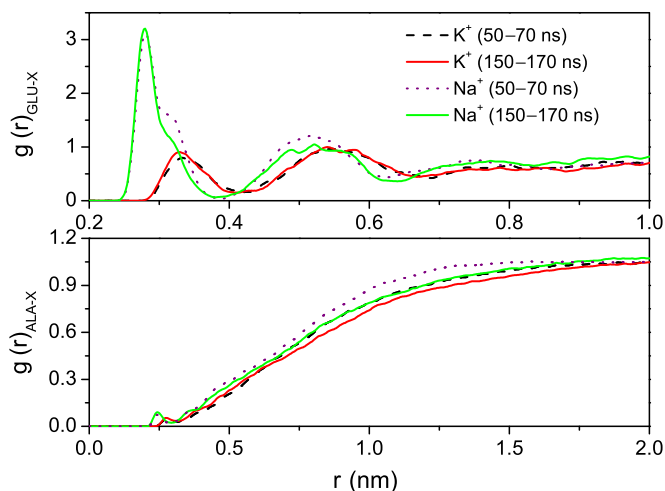


FIG. 8. (Color online) Time-dependent radial distribution functions of the different cations around polar and apolar residues. The 50–70 ns curves stand for the characteristics of the extended helix state while the 150–170 ns curves are for those of the α -helix state in the 0.5 Na⁺/0.5 K⁺ solution.

for the distribution of K⁺ and Na⁺, suggesting a particular residue-related ion cloud. It can be concluded that the cations rearrange near the protein surface in the 0.5 Na⁺/0.5 K⁺ solution and the excluded or included cations from inner or outer shells enhance the local crowding, resulting in a relative hydrophobic surrounding for the protein and shielding the peptide from solvation. The only collapsed state in the 0.5 Na⁺/0.5 K⁺ solution is also particularly different from the protein collapse in each case in the high-concentration urea/GdmCl mixture.

IV. CONCLUSION

Through the statistical analysis of conformational changes, the peptide in the 0.5 Na⁺/0.5 K⁺ solution was found at the most stabilized α -helix state. For other solutions, the peptide goes through a conformational transition to ringlike structures. The abundance of the ringlike structure is in accord with the greater probability of forming direct or indirect salt bridges for the Glu2-Lys6 pair in the 0.0 Na⁺/1.0 K⁺, 0.3 Na⁺/0.7 K⁺, and 1.0 Na⁺/0.0 K⁺ solutions, resulting in a straight unfolding process. The added single cations, especially for Na⁺, can consequently result in the conformational change to the ringlike structures. Because of this, the α -helix state is unstable in the 0.0 Na⁺/1.0 K⁺, 0.7 Na⁺/0.3 K⁺, and 1.0 Na⁺/0.0 K⁺ solutions. As shown in Fig. 9, the average helix probability (helicity) is also plotted. In 0.5 Na⁺/0.5 K⁺, the peptide has a remarkably higher helicity at residues

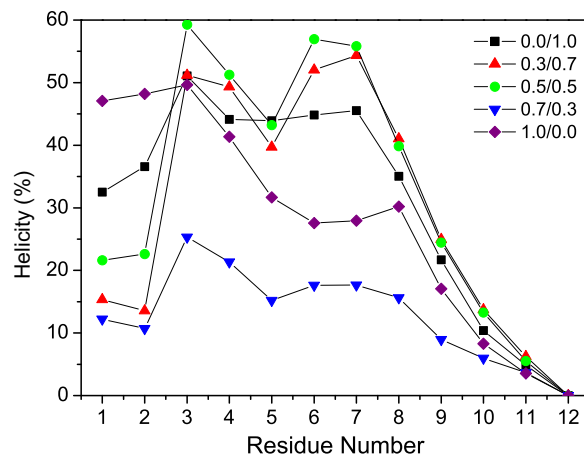


FIG. 9. (Color online) Average helix probability (helicity) of each residue in each case. The ACE and NH2 terminal groups are not included. The data are collected from 50 to 200 ns.

Ala3, Ala4, Lys6, and Glu7. The equally mixed Na⁺ and K⁺ not only ensure the larger helicity of the residues near by C terminal, but also keep the Glu7-Lys11 pair from forming ringlike structures. This significant stabilizing effect should be attributed to the higher chance of forming a direct or indirect salt bridge between Glu7⁻ and Lys11⁺ and the small probability of forming ringlike structures, protecting the backbone and keeping it from solvation.

Furthermore, the cations rearrange near the protein surface and the excluded or included cations from the inner or outer shells enhance the local crowding, resulting in a relative hydrophobic surrounding for the protein and shielding the peptide from solvation. This specific ion cloud is responsibility for the conformational transition from the extended α -helix to the α -helix state in the 0.5 Na⁺/0.5 K⁺ solution. This mechanism might be applied to artificially controlled specific protein folding or unfolding processes.

Our findings may be of general importance to the understanding of hybrid inorganic salt effects on protein secondary structure stability and may provide insight for further experiments on probing the specific cation effects on similar peptides.

ACKNOWLEDGMENTS

This work was supported by the National Natural Science Foundation of China under Grants No. 11025524 and No. 11161130520, the National Basic Research Program of China under Grant No. 2010CB832903, and the European Commissions 7th Framework Programme (FP7-PEOPLE-2010-IRSES) under Grant Agreement Project No. 269131.

- [1] J. A. McCammon and P. G. Wolynes, *Curr. Op. Struct. Biol.* **12**, 143 (2002).
- [2] Y. Zhou and M. Karplus, *Nature (London)* **401**, 400 (1999).
- [3] C. D. Snow, H. Nguyen, V. S. Pande, and M. Gruebele, *Nature (London)* **420**, 102 (2002).

- [4] X. Shen, B. Gu, S. A. Che, and F. S. Zhang, *J. Chem. Phys.* **135**, 034509 (2011).
- [5] F. Hirata, *Molecular Theory of Solvation* (Kluwer Academic, Dordrecht, 2003).
- [6] S. Pabit, H. Roder, and S. Hagen, *Biochemistry* **43**, 12532 (2004).

- [7] T. Cellmer, E. Henry, J. Hofrichter, and W. Eaton, *Proc. Natl. Acad. Sci. U.S.A.* **105**, 18320 (2008).
- [8] A. Möglich, K. Joder, and T. Kiefhaber, *Proc. Natl. Acad. Sci. U.S.A.* **103**, 12394 (2006).
- [9] B. Alberts, A. Johnson, J. Lewis, M. Raff, K. Roberts, and P. Walter, *Molecular Biology of the Cell* (Garland Science, New York, 2002).
- [10] L. Sun, X. Li, T. Hede, Y. Tu, C. Leck, and H. Ågren, *J. Phys. Chem. B* **116**, 3198 (2012).
- [11] Y. Q. Gao, *J. Phys. Chem. B* **115**, 12466 (2011).
- [12] V. F. Maxim, M. G. Jonathan, and S. Stephan, *J. Am. Chem. Soc.* **131**, 10854 (2009).
- [13] D. Joachim, *J. Am. Chem. Soc.* **130**, 14000 (2008).
- [14] J. S. Perkyns, Y. Y. Wang, and B. M. Pettitt, *J. Am. Chem. Soc.* **118**, 1164 (1996).
- [15] S. A. Hassan, *J. Phys. Chem. B* **109**, 21989 (2005).
- [16] T. Ghosh, A. Kalra, and S. Garde, *J. Phys. Chem. B* **109**, 642 (2005).
- [17] M. Kinoshita and Y. Haramo, *Bull. Chem. Soc. Jpn.* **78**, 1431 (2005).
- [18] T. Arakawa and S. N. Timasheff, *Biochemistry* **26**, 5147 (1987).
- [19] Y. Goto and S. Aimoto, *J. Mol. Biol.* **218**, 387 (1991).
- [20] R. A. Curtis, J. Ulrich, A. Montaser, J. M. Prausnitz, and H. W. Blanch, *Biotechnol. Bioeng.* **79**, 367 (2002).
- [21] S. Krimm, J. Mark, and M. Tiffany, *Biopolymers* **8**, 695 (1969).
- [22] M. Satoh, J. Komiyama, and T. Iijima, *Biophys. Chem.* **14**, 347 (1981).
- [23] P. Debye and E. Hückel, *Phys. Z.* **24**, 185 (1923).
- [24] W. B. Russel, D. A. Saville, and W. R. Schowalter, *Colloidal Dispersions* (Cambridge University Press, Cambridge, 1989).
- [25] V. F. Maxim, M. G. Jonathan, and S. Stephan, *Phys. Chem. Chem. Phys.* **9**, 5423 (2007).
- [26] K. D. Collins, *J. Biophys.* **72**, 65 (1997).
- [27] K. D. Collins, *Methods* **34**, 300 (2004).
- [28] R. L. Baldwin, *Biophys. J.* **71**, 2056 (1996).
- [29] M. G. Cacace, E. M. Landau, and J. J. Ramsden, *Q. Rev. Biophys.* **30**, 241 (1997).
- [30] G. Karlstrom, *Phys. Chem. Chem. Phys.* **5**, 3238 (2003).
- [31] S. Marqusee, V. H. Robbins, and R. L. Baldwin, *Proc. Natl. Acad. Sci. U.S.A.* **86**, 5286 (1989).
- [32] E. J. Spek, C. A. Olson, Z. Shi, and N. R. Kallenbach, *J. Am. Chem. Soc.* **121**, 5571 (1999).
- [33] A. Chakraborty, T. Kortemme, and R. L. Baldwin, *Protein Sci.* **3**, 843 (1994).
- [34] J. M. Scholtz, E. J. York, J. M. Stewart, and R. L. Baldwin, *J. Am. Chem. Soc.* **113**, 5102 (1991).
- [35] B. Gu, F. S. Zhang, Z. P. Wang, and H. Y. Zhou, *Phys. Rev. Lett.* **100**, 088104 (2008).
- [36] K. Lindorff-Larsen, N. Trbovic, P. Maragakis, S. Piana, and D. E. Shaw, *J. Am. Chem. Soc.* **134**, 3787 (2012).
- [37] T. E. Weksberg, G. C. Lynch, K. L. Krause, and B. M. Pettitt, *Biophys. J.* **92**, 3337 (2007).
- [38] F. C. Marincola, V. P. Denisov, and B. Halle, *J. Am. Chem. Soc.* **126**, 6739 (2004).
- [39] G. Schaftenaar and J. H. Noordik, *J. Comput. Aid. Mol. Des.* **14**, 123 (2000).
- [40] G. A. Kaminski, R. A. Friesner, J. Tirado-Rives, and W. L. Jorgensen, *J. Phys. Chem. B* **105**, 6474 (2001).
- [41] I. Nezbeda and J. Slovak, *Mol. Phys.* **90**, 353 (1997).
- [42] F. S. Zhang and R. M. Lynden-Bell, *Phys. Rev. E* **71**, 021502 (2005).
- [43] R. M. Lynden-Bell and P. G. Debenedetti, *J. Phys. Chem. B* **109**, 6527 (2005).
- [44] H. J. C. Berenden, D. Van Der Spoel, and R. Van Drunen, *Comput. Phys. Commun.* **91**, 43 (1995).
- [45] E. Lindahl, B. Hess, and D. van der Spoel, *J. Mol. Model* **7**, 306 (2001).
- [46] T. Darden, D. York, and L. Pedersen, *J. Chem. Phys.* **98**, 10089 (1993).
- [47] M. Tuckerman and B. J. Berne, *J. Chem. Phys.* **97**, 1989 (1992).
- [48] H. J. C. Berendsen, J. P. M. Postma, W. F. Van Gunsteren, A. Dinola, and J. R. Haak, *J. Chem. Phys.* **81**, 3684 (1984).
- [49] M. V. Fedorov, J. M. Goodman, and S. Schumm, *Phys. Chem. Chem. Phys.* **9**, 5423 (2007).
- [50] J. Dzubiella, *J. Phys. Chem. B* **114**, 7098 (2010).
- [51] R. H. Zhou, *Proc. Natl. Acad. Sci. U.S.A.* **100**, 13280 (2003).
- [52] S. Marqusee and R. L. Baldwin, *Proc. Natl. Acad. Sci. U.S.A.* **84**, 8898 (1987).
- [53] A. E. Garcia and K. Y. Sanbonmatsu, *Proc. Natl. Acad. Sci. U.S.A.* **99**, 2782 (2002).
- [54] T. Ghosh, S. Garde, and A. E. Garcia, *Biophys. J.* **85**, 3187 (2003).
- [55] Z. Xia, P. Das, E. I. Shakhnovich, and R. H. Zhou, *J. Am. Chem. Soc.* **134**, 18266 (2012).
- [56] W. F. Li, R. H. Zhou, and Y. G. Mu, *J. Phys. Chem. B* **116**, 1446 (2012).